Tino G. A. Heijmen, Robert Moszynski, Paul E. S. Wormer, Ad van der Avoird, Udo Buck, Christof Steinbach, and Jeremy M. Hutson

---

Articles you may be interested in

Communication: A benchmark-quality, full-dimensional ab initio potential energy surface for Ar-HOCO
J. Chem. Phys. 140, 151101 (2014); 10.1063/1.4871371

Ab initio potential energy surface and intermolecular vibrations of the naphthalene-argon van der Waals complex
J. Chem. Phys. 134, 064322 (2011); 10.1063/1.3555765

Inelastic collision cross sections of CH (X 2 Π) with He (1 S) on new ab initio surfaces
J. Chem. Phys. 118, 2206 (2003); 10.1063/1.1533010

Total differential cross sections and differential energy loss spectra for He–C 2 H 2 from an ab initio potential
J. Chem. Phys. 107, 7260 (1997); 10.1063/1.475321

Ab initio potential-energy surface and rotationally inelastic integral cross sections of the Ar–CH 4 complex
J. Chem. Phys. 107, 902 (1997); 10.1063/1.474388
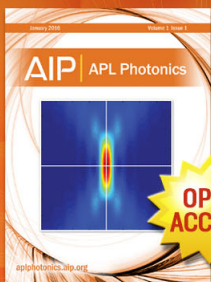
Total differential cross sections for Ar–CH$_4$ from an *ab initio* potential

Tino G. A. Heijmen
Institute of Theoretical Chemistry, NSR Center, University of Nijmegen, Toernooiveld 1, 6525 ED Nijmegen, The Netherlands

Robert Moszynski
Department of Chemistry, University of Warsaw, Pasteura 1, 02-093 Warsaw, Poland

Paul E. S. Wormer and Ad van der Avoird
Institute of Theoretical Chemistry, NSR Center, University of Nijmegen, Toernooiveld 1, 6525 ED Nijmegen, The Netherlands

Udo Buck and Christof Steinbach
Max-Planck-Institut für Strömungsforschung, Bunsenstraße 10, D-37073 Göttingen, Germany

Jeremy M. Hutson
Department of Chemistry, University of Durham, South Road, Durham DH1 3LE, United Kingdom

Total differential cross sections for the Ar–CH$_4$ scattering complex at $E_{CM}=90.1$ meV were obtained from converged close-coupling calculations based on a recent *ab initio* potential computed by symmetry-adapted perturbation theory (SAPT). Agreement with experiment is good, which demonstrates the accuracy of the SAPT potential. © *1998 American Institute of Physics.* [S0021-9606(98)00612-6]

I. INTRODUCTION

During the last few decades, a number of experimental and theoretical studies have been devoted to the rotationally elastic and inelastic scattering of Ar–CH$_4$. In their pioneering work[1–3] Secrest and coworkers applied both the close-coupling (CC) and coupled-states (CS) formalisms in the calculations of differential cross sections (DCS). Buck *et al.*[4] measured total differential cross sections in a crossed beam experiment at $E_{CM}=90.1$ meV. These results were used to derive an empirical potential of the Morse-spline-van der Waals type including the leading anisotropic contribution with tensor order $l=3$. Time-of-flight (TOF) spectra were reported[5] and compared with CS calculations that used the potential from Ref. 4. Total differential cross sections for Ar–CH$_4$ were also measured at slightly different collision energies.[6] Liuti *et al.*[7] reported total integral cross sections for rare gas–methane scattering as functions of the velocity. These data were used to further improve the isotropic term in the potential of Ref. 4.

Recently, we calculated an *ab initio* intermolecular potential energy surface for Ar–CH$_4$ using symmetry-adapted perturbation theory (SAPT).[8] After performing an analytical fit to the computed points, the long range dispersion and induction coefficients in the fit were replaced by coefficients calculated in a larger basis set. See Ref. 9 for a more detailed description of this asymptotic scaling procedure. We applied this *ab initio* potential in CC calculations of state-to-state integral cross sections for A, E, and T states of methane rotationally excited by collisions with argon. The results were generally in good agreement with experimental data.[10] The *ab initio* SAPT potential was also used to generate second virial coefficients for the Ar–CH$_4$ complex.[11] Virial co-

efficients computed from the asymptotically scaled potential were found to agree well with experiment, substantially better than those calculated from the original non-scaled potential.

In a previous work,[12] total differential cross sections and TOF spectra for He–C$_2$H$_2$ computed from a SAPT potential[13] were found to be in excellent agreement with experiment. In the current paper, we present total differential cross sections for Ar–CH$_4$, computed at the collision energy $E_{CM}=90.1$ meV, from converged CC scattering calculations. We compare the results obtained from the asymptotically scaled and the non-scaled SAPT potentials with the experimental data from Ref. 4.

II. COMPUTATIONAL DETAILS

The CC equations for atom–spherical top scattering were given in Refs. 8,14. The monomer wave functions for methane are expressed as linear combinations of symmetric top functions (normalized rotation matrix elements). The coefficients in these combinations are obtained by constructing and diagonalizing for each angular momentum j a rotational Hamiltonian matrix that includes the tetrahedral centrifugal distortion.[8,14] The following values were assigned to the rotational constant b, the centrifugal distortion constant d_j, and the tetrahedral centrifugal distortion constant d_t: $b=5.2410356$ cm^{-1}, $d_j=1.10864\times10^{-4}$ cm^{-1}, and $d_t=4.425\times10^{-6}$ cm^{-1}.[15] The CC equations were solved applying the modified log-derivative–Airy integrator.[16] The log-derivative propagator was used from $R_{min}=4.5$ bohr to $R_{mid}=15$ bohr with a constant step size corresponding to 5 steps per half wavelength for the open channel of highest kinetic energy in the asymptotic region. From R_{mid} to

$R_{max} = 100$ bohr the Airy propagator was used. Partial wave contributions with increasing values of the total angular momentum J were included until both the elastic and inelastic state-to-state cross sections were converged within 0.001 Å. With the asymptotically scaled potential, the highest values of J included for the A, E, and T symmetries were 309, 310, and 297, respectively. If the lengths of the partial wave expansions were smaller, the elastic contributions showed unphysical oscillations, especially at large angles. The angular basis contained all channels with monomer angular momentum j up to 14 inclusive. However, for the E and T symmetries the components with $J \geqslant 190$ and 182, respectively, were calculated in a basis including only channels with $j \leqslant 11$. The total number of channels for the bases with $j \leqslant 14$ and $j \leqslant 11$ were ≈ 385 and 190, respectively, for the E symmetry, and ≈ 560 and 290, respectively, for the T symmetry. Thus, decreasing the maximum value of the monomer angular momentum j from 14 to 11 caused the sizes of the basis sets to be reduced by approximately a factor of two. For the A symmetry, the total number of channels was ≈ 90. We tested that the deviations caused by the reduction of the monomer basis at large J were negligible. We performed additional calculations for the A states with the non-scaled potential and the same set of parameters. The highest value of J included was 307 in this case. The Ar–CH$_4$ interaction potential, which is a function of the distance R between the CH$_4$ center-of-mass (c.m.) and the Ar atom and of the polar angles (θ, ϕ) of the vector $\mathbf{R}$, was expanded in real combinations of spherical harmonics $Y_m^l(\theta, \phi)$ with $l \leqslant 18$. The expansion coefficients were computed by means of 25-point Gauss-Legendre and Gauss-Chebyshev quadratures in θ and ϕ, respectively. The reduced mass of Ar–CH$_4$ is 11.441478 amu.[17] The integration parameters, the size of the monomer basis, the number of partial waves, and the length of the expansion of the potential were chosen such that the state-to-state cross sections were converged within 1% at worst. All scattering calculations were performed using the MOLSCAT system of codes.[18] Differential cross sections in the c.m. frame were generated from the calculated S-matrix elements using the DCS program.[19] This program was extended such that it can be applied to atom–spherical top systems. The c.m. scattering angle Θ_{CM} was varied from 0° to 180° with steps of 0.5°. It was assumed that initially the methane molecules are in the lowest rotational state permitted for each of the symmetry types, i.e., $j'' = 0$, 1, and 2 for A, T, and E symmetries, respectively.

In order to compare the *ab initio* total differential cross sections, summed over all elastic and inelastic channels, with experiment, the calculated values were transformed from the c.m. frame to the laboratory-fixed (lab) frame and averaged over the velocity and angular distributions of the methane and argon beams. Furthermore, corrections were made for the energy response and physical size of the detector. The averaging procedure is described in detail elsewhere.[20] The key parameters are the full width at half maximum of the c.m. angular and velocity distributions, $\delta = 1.46°$ and $\Delta g/g = 0.13$, respectively. They are calculated using a Monte–Carlo procedure with the quantities mentioned above as input information. The actual calculations are then performed

(a)

(b)
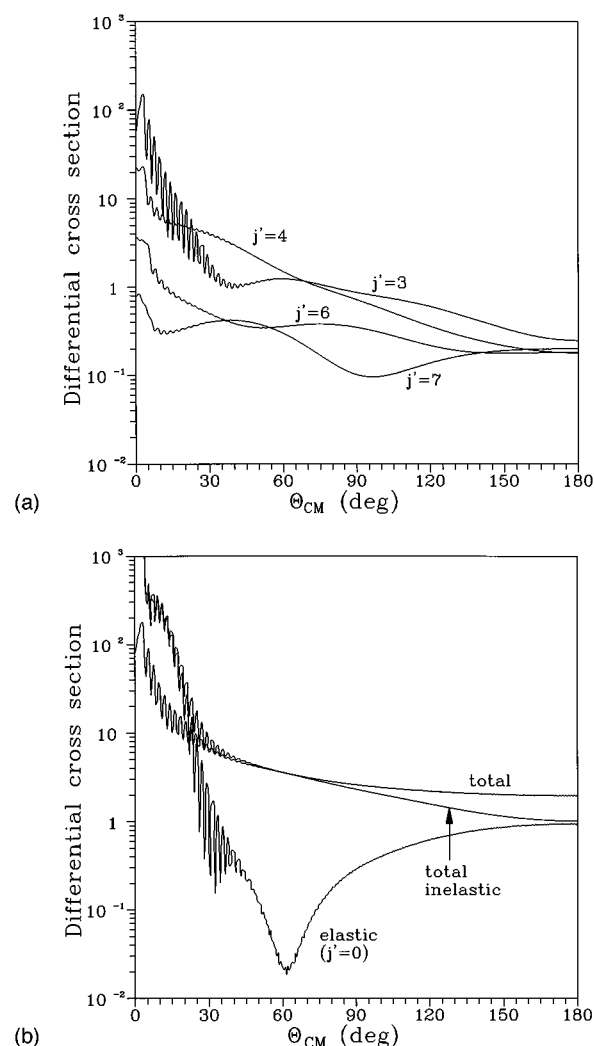
FIG. 1. State-to-state inelastic (a) and elastic, total inelastic, and total (b) differential cross sections for the A symmetries of Ar–CH$_4$ calculated with the asymptotically scaled SAPT potential as functions of the c.m. angle. The molecular rotational quantum numbers of the final states are indicated.

on a 12×12 point grid in the two variables. The energy dependence of the cross sections is explicitly taken into account with the help of a scaling law[21] which has been checked against exact calculations.

III. RESULTS AND DISCUSSION

Figures 1(a) and 1(b) depict the state-to-state, total inelastic, and total differential cross sections for the A symmetries of Ar–CH$_4$ as functions of the c.m. angle Θ_{CM}. The same results for the T species are presented in Figs. 2(a) and 2(b) and for the E states in Figs. 3(a) and 3(b). Only cross sections for the transitions with $j' \leqslant 7$ are shown (j' denotes here the rotational quantum number of the final state). Cross sections with higher j' are not reported since their contribution to the total differential cross sections is very small. An inspection of these figures shows that at small angles the elastic component dominates the total differential cross sections. At larger angles the inelastic transitions become increasingly important, especially for the A and T symmetries. For these symmetries the elastic term has a deep minimum
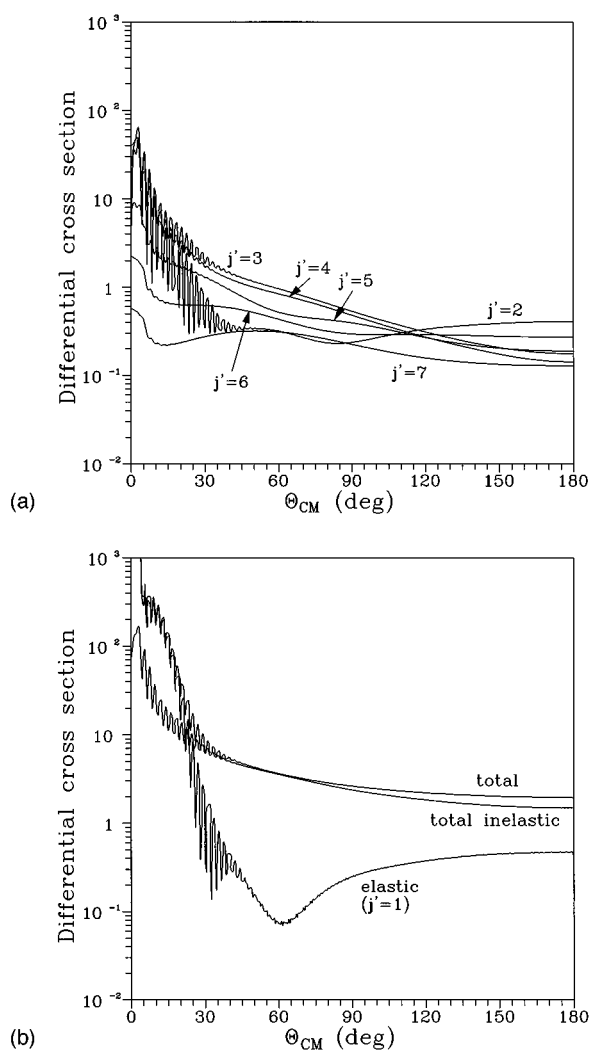
FIG. 2. State-to-state inelastic (a) and elastic, total inelastic, and total (b) differential cross sections for the T symmetries of Ar–CH_4 calculated with the asymptotically scaled SAPT potential as functions of the c.m. angle. The molecular rotational quantum numbers of the final states are indicated.

FIG. 3. State-to-state inelastic (a) and elastic, total inelastic, and total (b) differential cross sections for the E symmetries of Ar–CH_4 calculated with the asymptotically scaled SAPT potential as functions of the c.m. angle. The molecular rotational quantum numbers of the final states are indicated.

around $\Theta_{CM} = 60°$. It is interesting to note that although various state-to-state differential cross sections show very different dependence on the c.m. deflection angle, the total cross sections (i.e., the cross sections summed over the elastic and all inelastic channels) are almost identical.

The theoretical total differential cross sections for the A states of Ar–CH_4, transformed to the lab frame and averaged over the experimental conditions, are reported as a function of the laboratory angle in Fig. 4. It was essential that different inelastic contributions were transformed individually, since they have different final velocities. The use of the purely elastic transformation would substantially underestimate the theoretical differential cross sections at large lab angles. The experimental cross sections from Ref. 4 are displayed in this figure as well. In order to remove the strong angular dependence of the elastic differential cross section the data are multiplied by $\Theta^{7/3}$. Although the state-to-state differential cross sections for the E and T states of Ar–CH_4 are different from those of the A species (cf. Figs. 1–3), the total differential cross sections in the lab frame were found to

be almost identical. Therefore, these results are not shown. The position of the maximum of the total differential cross sections, the rainbow angle, is very well reproduced, but the slope of the theoretical curve beyond the rainbow angle is somewhat different from experiment. These two features of the total differential cross sections are mainly sensitive to the well depth of the potential, so the results presented in Fig. 4 suggest that the well depth of the *ab initio* potential is underestimated, but only by a very minor amount. Furthermore, the positions and amplitudes of the diffraction oscillations, which modulate the maximum of the curve, agree well with experiment. This result indicates that both the onset of the repulsive wall (R_0) and the anisotropy of the minimum distance $R_m(\Theta)$ of the potential are realistic. On the other hand, the coarse structure amplitude of the curve, which represents the rainbow maximum, slightly deviates from the experimental data. Test calculations of the averaging process show that the rainbow amplitude is not influenced by small changes of the resolution.

A possible reason for such a behavior could be too weak
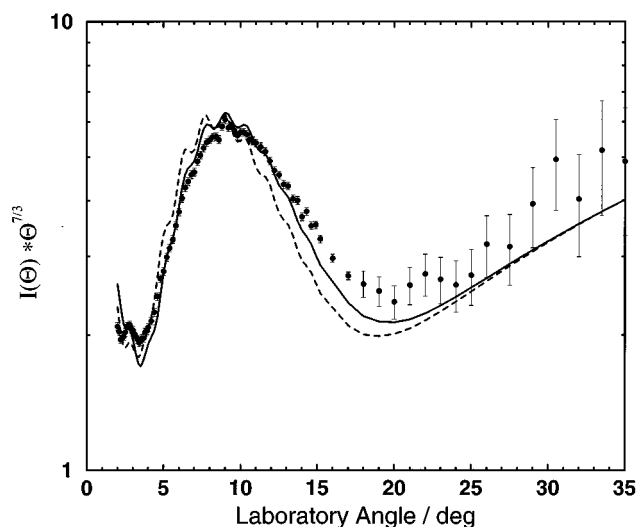
FIG. 4. Total differential cross sections (multiplied by $\Theta^{7/3}$) computed from the asymptotically scaled SAPT potential (solid line) and the non-scaled SAPT potential (dashed line) as functions of the lab angle. Circles denote experimental data from Ref. 4, the error bars represent ± 1 standard deviation of the mean.

FIG. 5. Total differential cross sections (multiplied by $\Theta^{7/3}$) computed from the semiempirical $V_0^c + V_3^c$ potential of Ref. 4 as functions of the lab angle. Circles denote experimental data from Ref. 4, the error bars represent ± 1 standard deviation of the mean.

a damping of the rainbow amplitude due to the anisotropy of the well depth. However, a careful inspection of the total differential cross sections in the rainbow region shows that they are completely dominated by the elastic contributions. This is also reflected in the potential terms in the attractive part near the inflection point which is the part of the potential that is most sensitively probed in rainbow scattering. Here V_0 is much larger than the anisotropic V_3 and V_4 terms.[8] Therefore we attribute the small discrepancy in the rainbow amplitude to a small error in the shape of the potential near the inflection point: the rainbow impact parameter is slightly too large, which influences the rainbow amplitude.[22] Indeed the best fit isotropic potentials of Refs. 4, 7 exhibit smaller rainbow impact parameters and thus slightly smaller amplitudes.

For comparison, we have plotted in Fig. 5 the total differential cross sections for the *A* states of Ar–CH$_4$, calculated from the semiempirical potential $V_0^c + V_3^c$ reported by Buck *et al.*[4] This figure is not identical with Fig. 8 of Ref. 4, which was obtained from the same potential, because in the present work we applied the close-coupling instead of the coupled-states formalism and did not retransform the results to the c.m. frame. The agreement of the present curve with experiment is worse between 5° and 6° (lab angles), the same up to 20°, and better for larger angles. The *ab initio* results of Fig. 4 agree somewhat better with experiment than the semiempirical results for angles smaller than 12°, somewhat worse between 12° and 23°, and are comparable for larger angles. On the average, agreement with the experimental results is equally good for the SAPT potential and for the semiempirical potential of Ref. 4 that was mainly fitted to these data.

Also reported in Fig. 4 are the theoretical total differential cross sections calculated from the non-scaled SAPT potential. An inspection of the figure shows that the agreement
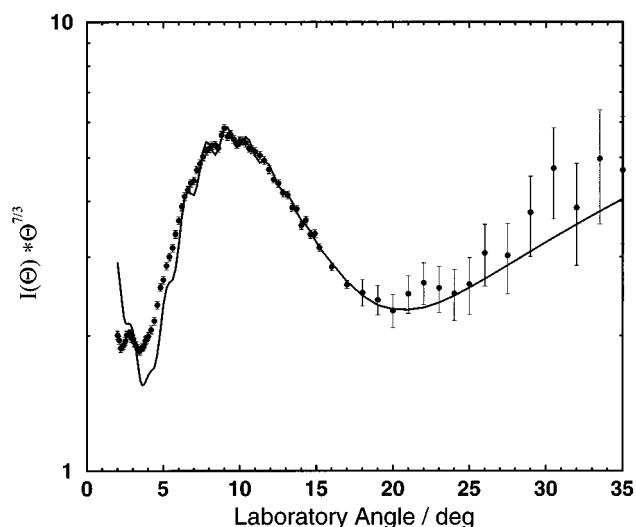
with experiment[4] is considerably worse. The predicted rainbow angle is too small, indicating that the well of this potential is too shallow. A change in the well depth of the potential also affects the onset of the repulsive wall. Consequently, the oscillations on the curve for the non-scaled potential in Fig. 4 are slightly out of phase with respect to the experimental data. A similar result concerning the well depth was found from the analysis of the second virial coefficients calculated with the asymptotically scaled and the non-scaled SAPT potentials.[11]

We conclude that the asymptotically scaled SAPT potential reported in Ref. 8 is able to reproduce well the total differential cross sections for Ar–CH$_4$. The only deviation from experiment is in the rainbow amplitudes suggesting that there are small inaccuracies in the shape of the potential near the inflection point. The well depth of the potential, however, is very realistic, since the position of the rainbow angle is accurately reproduced. Comparison with the results obtained from the semiempirical potential of Ref. 4, which was fitted to the measured differential cross sections, shows that the results from the SAPT potential agree about equally well with these experimental data. Work on the application of this *ab initio* potential to generate the infrared spectrum of the Ar–CH$_4$ complex in the region of the ν_3 mode is in progress. Comparison with the experimental spectrum[23–25] will provide a further check of the accuracy of the potential.

ACKNOWLEDGMENTS

[1] T. G. Heil and D. Secrest, J. Chem. Phys. **69**, 219 (1978).
[2] L. N. Smith, D. J. Malik, and D. Secrest, J. Chem. Phys. **71**, 4502 (1979).

[3] L. N. Smith and D. Secrest, J. Chem. Phys. **74**, 3882 (1981).

[4] U. Buck, J. Schleusener, D. J. Malik, and D. Secrest, J. Chem. Phys. **74**, 1707 (1981).

[5] U. Buck, A. Kohlhase, T. Phillips, and D. Secrest, Chem. Phys. Lett. **98**, 199 (1983).

[6] M. J. O'Loughlin, B. P. Reid, and R. K. Sparks, J. Chem. Phys. **83**, 5647 (1985).

[7] G. Liuti, F. Pirani, U. Buck, and B. Schmidt, Chem. Phys. **126**, 1 (1988).

[8] T. G. A. Heijmen, T. Korona, R. Moszynski, P. E. S. Wormer, and A. van der Avoird, J. Chem. Phys. **107**, 902 (1997).

[9] R. Moszynski, P. E. S. Wormer, B. Jeziorski, and A. van der Avoird, J. Chem. Phys. **101**, 2811 (1994).

[10] W. B. Chapman, A. Schiffman, J. M. Hutson, and D. J. Nesbit, J. Chem. Phys. **105**, 3497 (1996).

[11] R. Moszynski, T. Korona, T. G. A. Heijmen, P. E. S. Wormer, A. van der Avoird, and B. Schramm, Pol. J. Chem. (in press).

[12] T. G. A. Heijmen, R. Moszynski, P. E. S. Wormer, A. van der Avoird, U. Buck, I. Ettischer, and R. Krohne, J. Chem. Phys. **107**, 7260 (1997).

[13] R. Moszynski, P. E. S. Wormer, and A. van der Avoird, J. Chem. Phys. **102**, 8385 (1995).

[14] J. M. Hutson and A. E. Thornley, J. Chem. Phys. **100**, 2505 (1994).

[15] G. Tarrago, M. Dang-Nhu, G. Poussigue, G. Guelachvili, and C. Amoit, J. Mol. Spectrosc. **57**, 246 (1975).

[16] M. H. Alexander and D. E. Manolopoulos, J. Chem. Phys. **86**, 2044 (1987).

[17] *Handbook of Chemistry and Physics*, edited by R. C. Weast and M. J. Asth, (CRC, Boca Raton, 1981).

[18] J. M. Hutson and S. Green, MOLSCAT computer code, version 14 (1994), distributed by Collaborative Computational Project No. 6 of the Engineering and Physical Sciences Research Council (UK).

[19] S. Green and J. M. Hutson, DCS computer code, version 2.0 (1996), distributed by Collaborative Computational Project No. 6 of the Engineering and Physical Sciences Research Council (UK).

[20] U. Buck, in *Atomic and Molecular Beam Methods*, edited by G. Scoles (Oxford University Press, Oxford, 1988), Vol. 1, Chap. 20.3.

[21] M. Shapiro, R. B. Gerber, U. Buck, and J. Schleusener, J. Chem. Phys. **67**, 3570 (1977).

[22] H. Pauly, in *Atom-Molecule Collision Theory*, edited by R.B. Bernstein (Plenum, New York, 1979), p. 111.

[23] A. R. W. McKellar, Faraday Discuss. Chem. Soc. **97**, 69 (1994).

[24] R. E. Miller, Faraday Discuss. Chem. Soc. **97**, 177 (1994).

[25] D. J. Nesbitt, Faraday Discuss. Chem. Soc. **97**, 175 (1994).